AIRFLOW AND RADON TRANSPORT MODELING IN FOUR LARGE BUILDINGS

Jin B. Fang, Ph.D.

Andrew K. Persily, Ph.D.
Member ASHRAE

ABSTRACT

Computer simulations of multizone airflow and contaminant transport were performed in four large buildings using the program CONTAM88. This paper describes the physical characteristics of the buildings and their idealizations as multizone building airflow systems. These buildings include a twelve-story multifamily residential building, a five-story mechanically ventilated office building with an atrium, a seven-story mechanically ventilated office building with an underground parking garage, and a one-story school building. The air change rates and interzonal airflows of these buildings are predicted for a range of wind speeds, indoor-outdoor temperature differences, and percentages of outdoor air intake in the supply air. Simulations of radon transport were also performed in the buildings to investigate the effects of indoor-outdoor temperature difference and wind speed on indoor radon concentrations.

INTRODUCTION

Infiltration and exfiltration of air through exterior envelopes and interzonal airflow rates in buildings affect whole building ventilation rates, outdoor airflow rates to individual rooms, concentration levels of airborne contaminants, heating and cooling loads, and smoke movement in the case of fire. Air movement and convective contaminant transport within multizone buildings are caused by pressure differences across openings in exterior walls and in partitions between individual zones. These pressure differences are caused by wind, thermal buoyancy, and airflows from mechanical ventilation systems. For a building with known air leakage characteristics, ventilation system airflow rates, weather conditions, and pollutant source strengths, multi-zone airflow and contaminant transport models can predict the airflow rates from one zone to another (including to and from the outdoors) and the contaminant levels in each zone.

Several models have been developed for predicting airflow, contaminant dispersal, and fire-induced smoke movement in multi-zone buildings. These multizone airflow and contaminant dispersal models were reviewed by Feustel and Kendon (1985), Feustel and Dieris (1992), Austin et al. (1992), Haghighat (1989), and Said (1988). These models use a network approach to obtain a set of nonlinear equations derived from a mass balance at each node and an iterative solution technique based on the Newton-Raphson method to solve for the pressure at each node. These pressures are then used to calculate the steady-state airflow rates to and from each zone based on the given leakage values. Using these airflow rates and pollutant source strengths and information on other pollutant transport mechanisms, these programs calculate contaminant concentrations in each building zone.

Multizone airflow and contaminant dispersal models can be used to investigate air movement in multistory buildings, to predict interzonal airflow patterns and zonal contaminant concentration levels, and to evaluate the performance of the building ventilation systems under different operating conditions. Predicted air leakage rates can also be used to assess the effectiveness of interior doors and walls as barriers to contaminants or smoke flow and to design contaminant or smoke control systems. Modeling can also be useful to designers, builders, and code enforcement officials to predict whether the performance of a building will fulfill local fire, energy, and indoor air quality codes and standards.

Despite the potential usefulness of these models, the validity of their predictions has not yet been established. Model validation is critical because it is very easy to run a large number of simulations for a given building and then draw conclusions about the impact of various parameters on ventilation and indoor air quality. One of the more important issues related to model validation is the value of the various model inputs since the validity of the model output is a function of the appropriateness of the input values. Multizone airflow models require information on the building being modeled, including physical dimensions of the building, airflow resistances of the airflow paths, the configuration of mechanical ventilation systems, ventilation system airflow rates, wind pressure coefficients on the building facade, and ambient weather data. Contaminant dispersal analysis requires additional information, including contaminant source strengths, source removal rates from indoor sinks, filter efficiencies, and outdoor contaminant concentrations. However, when performing multi-zone airflow and contaminant dispersal analysis for a given building, there is generally only limited information available on the required inputs.

Another issue related to the validity of the model predictions is how a multizone building is idealized within the model. An idealization of a multizone building refers to its representation as a multizone airflow system in a manner

Jin B. Fang is a mechanical engineer and **Andrew K. Persily** is a group leader in the Building and Fire Research Laboratory, National Institute of Standards and Technology, Gaithersburg, MD.

that captures the important features of the building and the airflow and contaminant dispersal phenomena being studied. The idealization of a multizone building depends on the building layout, the ventilation system configuration, and the objective of the modeling effort. A very complex building need not be modeled to include every building zone and leakage path but in some situations can be idealized as a much simpler system with a smaller number of zones. Building idealization for airflow modeling has not received a great deal of attention in the literature on airflow modeling, and no general rules are available to guide the modeler.

The objective of this paper is to introduce the reader to the capabilities of multizone airflow and contaminant dispersal modeling. In addition, four large buildings that are available for indoor air quality analysis are presented along with sample results of simulations of airflow and radon transport in these buildings. The four buildings include a twelve-story apartment building, a five-story mechanically ventilated office building with an atrium, a seven-story mechanically ventilated office building with an underground parking garage, and a one-story school building. The first section of the paper describes the computer program CONTAM88 (Grot 1991) and its companion program NBSAVIS, including the assumptions employed, the inputs required, and the outputs of the program. The physical characteristics of the four buildings and their multizone idealizations in the model are described in the next section. The third section presents sample simulation results for the four buildings. The results show the effects of wind speed, indoor-outdoor temperature difference, and percent outdoor air intake rate on the calculated building air change rates. In addition, radon entry and transport are modeled for each of the buildings, and the effects of weather conditions and ventilation system operation on radon concentration in these buildings is examined. The paper also includes an appendix containing a building component air leakage data base for large commercial buildings. Additional details on the building airflows simulations are contained in Fang and Persily (1994).

CONTAM88

CONTAM88 was developed to enable multizone airflow and contaminant dispersal modeling in buildings (Grot 1991). This model assumes that a building can be idealized as a number of well-mixed zones that exchange air with each other and the outdoors through air leakage paths and ventilation systems. The computer code predicts air movement and contaminant concentration levels within a multizone building given the leakage characteristics of the openings to the outdoors and between zones, ventilation system airflows, weather conditions, contaminant sources and sinks, and wind pressure coefficients for the building exterior surfaces. Building surface wind pressure coefficients, if not given, can also be specified by a default algorithm within the code. The code is a combination of two previously developed programs: AIRMOV (Walton 1983, 1984), which performs network airflow analysis, and CONTAM87 (Axley 1988), which simulates contaminant dispersal in multizone systems.

A companion program to CONTAM88, called NBSAVIS, is a menu-driven preprocessor for creating building descriptions and data input files that are used by CONTAM88. These input files are used to calculate the airflow rates and contaminant concentration levels in buildings using the CONTAM88 program in conjunction with a weather data file and a program parameter file. The CONTAM88 code is capable of calculating steady-state airflow rates and both steady-state and transient contaminant concentrations.

Since the simulations in this study were performed, an updated version of the CONTAM program has been released. This new version, CONTAM93 (Walton 1994), has essentially the same airflow and contaminant dispersal simulation capabilities as CONTAM88. However, the new program employs a graphical interface to describe the building, input data, and display the simulation results.

BUILDING DESCRIPTIONS

This section describes the four buildings that were modeled, including their idealizations as multizone systems and the leakage values used to describe the airflow paths between the zones. While the office buildings and school are based on real buildings, only the exterior wall leakage value of Office Building No. 1 is based on an actual measurement. All other leakage values were based on data in Appendix A of this paper and the *ASHRAE Fundamentals* (1993). When a range of values was available for the leakage of a particular component, a value in middle of the range was used. The leakage values were not selected to represent specific or typical buildings, but the building airflow simulations are expected to yield reasonable results.

Apartment Building

The apartment building being modeled consists of 12 stories and a basement and is based on a simplified building representation employed previously to model air and radon transport in a multistory residential building (Persily 1993). The apartment building has horizontal dimensions of 30 m by 22.5 m, a ceiling height of 2.5 m on each floor, a roof height of 30.5 m above grade, and a basement 2 m below grade. A typical floor plan of this building is shown in Figure 1.

Each typical story (second through twelfth floors) of the building has four apartments, with two on each side of a central hall. The first floor contains a large lobby with a main entrance at the center of the west exterior wall and two apartment units on the east side. The building has an eleva-

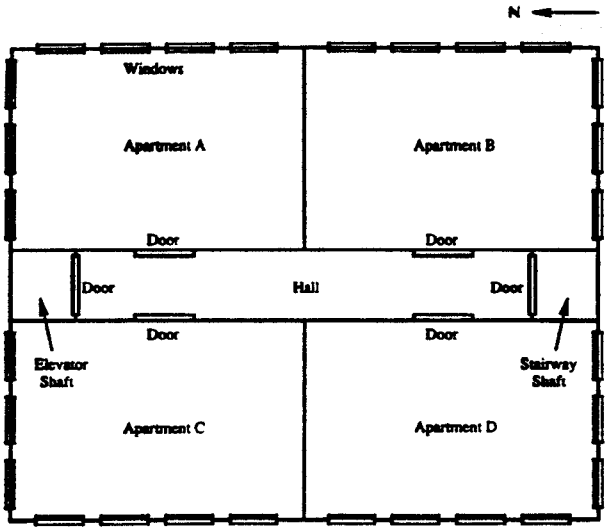

Figure 1: Typical floor plan of apartment building.

tor shaft and a stairwell located at the ends of the hall. Both the elevator and stairwell shafts extend from the basement to the roof and have horizontal dimensions of 2.5 m by 2 m. The hall is 26 m by 2.5 m. The basement has no interior partitions, except for the walls of the stair and elevator shafts. Closed doors connect the hall to each apartment and the halls and the basement to the elevator and stairwell shafts. The shafts are modeled as a series of vertically connected single-story zones. These shaft zones are connected by openings with a cross-sectional area equal to the cross-sectional area of the shafts. Other models are available for shafts that account for the airflow resistance within them (Ackakji and Tamura 1988). The use of these other models is more critical when there are large airflow rates in the shafts, such as during the operation of smoke control systems. Two exterior doors are located at the roof levels of the stairwell and elevator shafts. There are four windows on the long wall and three on the short wall of each apartment.

The leakage values used for the major building components are as follows:

Exterior walls	3.0 cm^2/m^2
Entrance door	58 cm^2
Apartment windows	7.5 cm^2
Interior walls	2.0 cm^2/m^2
Interior floors	0.5 cm^2/m^2
Apartment doors	75 cm^2
Elevator and stairway doors	150 cm^2

All leakage areas are based on a reference pressure of 4 Pa and a discharge coefficient of 1.0. All leakage paths are characterized by a pressure exponent of 0.6. The representation of this apartment building consists of 87 zones and 1,233 openings.

Office Building No. 1

The first of two office buildings that were modeled is a seven-story mechanically ventilated building with an atrium. This building is based on an office building located in Overland, Missouri, that was the subject of a study of building ventilation and indoor air quality (Persily et al. 1991, 1992). The building consists of five floors above grade and two floors, levels B1 and B2, below grade. A schematic floor plan of level 5 is shown in Figure 2. The main entrance of the building is located on the first floor, and a penthouse is situated on the south corner of the rooftop. The building is square in shape and has a square atrium in its center extending from the first floor to the roof. The building has overall dimensions of 74.4 m on a side, a ceiling height of 3.35 m on each floor, a total floor area of about 32,500 m^2, and a volume of about 122,000 m^3. Stairways are located in each corner of the building, and there are six passenger elevators and a freight elevator located in the south corner. A detailed description of the actual building, including floor plans for all levels, is given in Persily et al. (1991).

The building has a decentralized ventilation system with two variable-air-volume air-handling systems serving each floor and one additional system serving the atrium. Two toilet fans are located on the roof and serve each floor through a common exhaust duct. Return air from the occupied spaces flows through a return air plenum above the

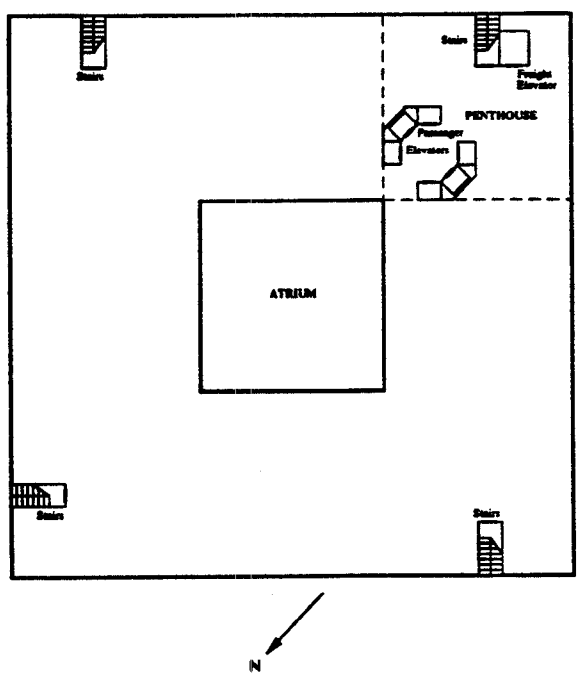

Figure 2: Level-5 floor plan of office building No. 1.

suspended ceiling and back to the air handlers where it is either recirculated into the supply air or exhausted to the outdoors. The mechanical system airflow rates used in the simulations are given in Fang and Persily (1992).

The following air leakage values were used in airflow calculations for the major components of the building. They are all based on a reference pressure of 4 Pa, a discharge coefficient of 1.0, and a pressure exponent of 0.6.

Exterior walls	5.2 cm^2/m^2
Entrance door	58 cm^2
Interior floors	0.4 cm^2/m^2
Interior doors	
Passenger elevator	200 cm^2
Stairway	174 cm^2
Freight elevator	430 cm^2

The leakage value for the exterior walls is based on the results of a whole building pressure test of the building (Persily et al. 1991). A leakage area of 40 cm^2 is specified for cable openings at the top of the elevator shaft in the penthouse. The stairway and elevator shafts are modeled by a series of vertically connected zones, one for each floor. These shaft zones are connected by an opening with an area equal to the cross-sectional area of the shaft. The space on each building floor is modeled as two zones, consisting of one zone below the suspended ceiling and another zone above the suspended ceiling. The leakage area of the suspended ceiling is 35 cm^2/m^2. This office building is represented by 66 zones and 746 openings.

Each of the 15 air-handling systems (two per floor plus the atrium system) is modeled within CONTAM88 as two HVAC systems, one supply and one return system. Supply airflow rates are specified from each supply air-handling system to the zone below the suspended ceiling. Return airflow rates are specified from the zone above the suspended ceiling to each supply system in order to account for recirculated return air. Another return airflow rate is specified from the zone above the ceiling to the return HVAC system to account for return air that is exhausted to the outdoors. For the supply systems, any difference between the airflow rate of recirculated return air and supply air is made up with outdoor air intake. By adjusting the airflow rates of return air to the supply and return HVAC systems, one can modulate the outdoor airflow rate brought into the building. Three levels of outdoor air intake were applied to Office Building No. 1: 100% outdoor air intake, 50% outdoor air intake, and the minimum design level of outdoor air intake.

Office Building No. 2

This mechanically ventilated office building has seven stories above grade, one story below grade, and a two-story underground parking garage. It is based on an office building in Portland, Oregon, that was the subject of a study of ventilation and indoor air quality (Grot et al. 1989; Dols and Persily 1992). A schematic elevation of the building is shown in Figure 3. The building has a main entrance and reception area on the first floor and a loading dock on the first below-grade level. An underground parking garage is located on the next two below-grade levels. The building mechanical equipment is located in a rooftop penthouse.

The building has a conditioned floor area of about 42,900 m^2 and a building volume of approximately 183,600 m^3. Eight passenger elevators and a freight elevator are located on the east side of the building. Stairways that provide access to all ten building floors are located on both the east and west sides of the building. Another stairway is located on the west side of the building and links only the seven levels above grade. These stairways are connected to the occupied areas of the building by closed doors. The two-story parking garage is connected to the occupied spaces by two stairways and four passenger elevators.

There are three variable-air-volume air handlers in the penthouse mechanical room that serve all seven above-grade floors. These air handlers serve the east, west, and center of the building. There are several separate air-handling units located on and serving the B1 level. Two toilet fans are located on the roof and serve each floor through a common duct. The underground garage has four exhaust fans. The mechanical system airflow rates used in the simulations are given in Fang and Persily (1994).

The leakage values for the major building components in Office Building No.2 are as follows:

Exterior walls	2.0 cm^2/m^2
Entrance door	31 cm^2
Loading dock door	58 cm^2
Garage door	150,000 cm^2
Interior floors	0.4 cm^2/m^2
Interior doors	
Passenger elevator	200 cm^2
Stairway	200 cm^2
Freight elevator	300 cm^2

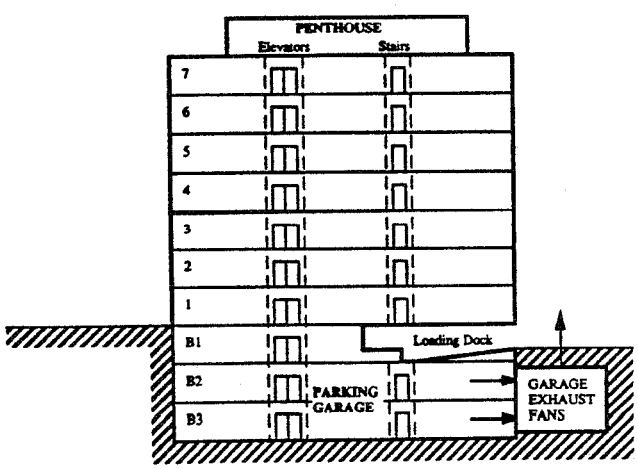

Figure 3: Schematic elevation of office building No.2.

These leakage areas are all based on a reference pressure of 4 Pa, a discharge coefficient of 1.0, and a pressure exponent of 0.6.

The stairway and elevator shafts are modeled by a series of vertically connected zones, one for each floor. These shaft zones are connected by an opening with an area equal to the cross-sectional area of the shaft. The space on each building floor is modeled as two zones, consisting of one zone below the suspended ceiling and another zone above the suspended ceiling. The parking garage is modeled as two zones, one for each level, which are horizontally divided by a floor. The upper level of the garage has a large door open to the exterior and is connected to the lower level through a 7.6 m by 3.1 m opening in the floor. The representation of this office building contains 77 zones and 660 openings.

Each of the three main air-handling systems is modeled as two HVAC systems, one supply and one return system. All of the air handlers serving level B1 are modeled with another supply and return system. Supply airflow rates are specified from each supply air-handling system to the zone below the suspended ceiling. Return airflow rates are specified from the zone above the suspended ceiling to each supply system in order to account for recirculated return air. Another return airflow rate is specified from the zone above the ceiling to the return HVAC system to account for return air that is exhausted to the outdoors. For the supply systems, any difference between the airflow rate of recirculated return air and supply air is made up with outdoor air intake. By adjusting the airflow rates of return air to the supply and return HVAC systems, one can modulate the outdoor airflow rate brought into the building. Three levels of outdoor air intake were applied to Office Building No. 2: 100% outdoor air intake, 50% outdoor air intake, and the minimum design level of outdoor air intake.

School Building

The school building is a one-story, mechanically ventilated building consisting of classrooms, conference rooms, offices, storage rooms, corridors, toilets, a kitchen, an all-purpose room, and a boiler room. A floor plan of the school is shown in Figure 4. The numbers in the figure refer to the zone numbers. The building has a 12.5 m × 32.8 m central courtyard and overall dimensions of approximately 66 m × 72 m. The total floor area of the building is about 3,990 m^2, and the building volume is approximately 15,050 m^3.

The ventilation system in this building consists of a combination of unit ventilators, supply air handlers, and exhaust fans. Forty-three individual unit ventilators are mounted in the exterior walls of the classrooms and several office and storage rooms. An individual supply air handler serves the general office space. The building also has nine ducted exhaust systems that serve various combinations of rooms in the building. There are 16 local exhaust fans that

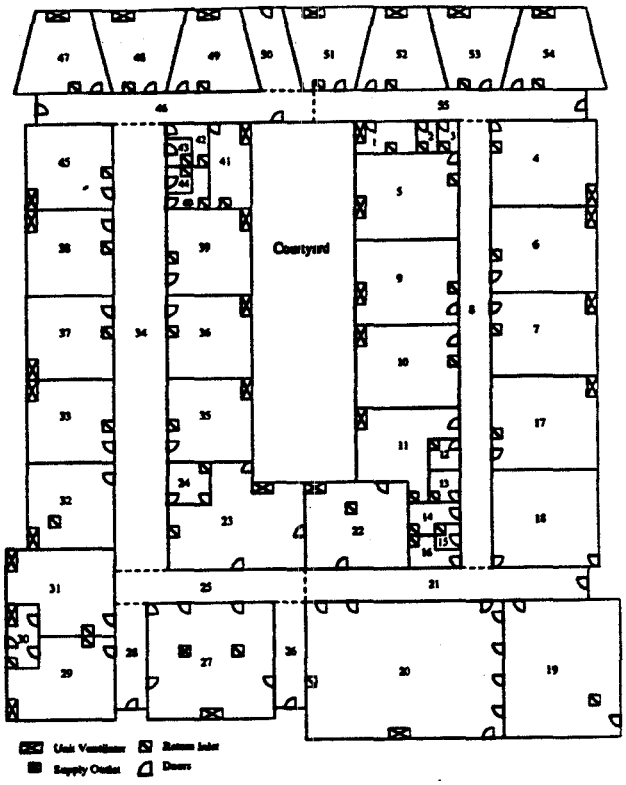

Figure 4: Floor plan of school building.

serve the kitchen, general office space, and conference/storage rooms. The total supply airflow capacity of the building is 17.5 m^3/s, which corresponds to an air change rate of 3.92 ACH. The outdoor airflow rate is 4.38 m^3/s, corresponding to 25% outdoor air intake. The total exhaust airflow capacity is 12.5 m^3/s. Therefore, there is an excess of mechanical exhaust over outdoor air intake in this building. Additional information on the mechanical system airflow rates used in the simulations is given in Fang and Persily (1994).

The leakage values for the major building components in the school building are as follows:

Exterior walls	
Masonry	2.9 cm^2/m^2
Window	2.0 cm^2/m^2
Exterior doors	29 cm^2
Windows	3.8 cm^2
Interior walls	2.0 cm^2/m^2
Interior doors	75 cm^2

These leakage areas are all based on a reference pressure of 4 Pa, a discharge coefficient of 1.0, and a pressure exponent of 0.6.

In the computer simulations, the unit ventilators are modeled as a fixed outdoor flow rate to each individual room. The supply airflow to general office space is also modeled as a fixed flow. The nine ducted exhaust systems are modeled as HVAC systems within the CONTAM88 program, with return vents located in each room served by the

individual systems. The local exhaust fans serving the kitchen and other rooms are modeled as fixed exhaust airflows. The representation of this school building contains 63 zones and 629 openings.

Radon Modeling

This section describes how radon entry and transport were modeled in the four buildings. While there has been significant research and other activity related to radon in single-family residential buildings, relatively little work has been done in large buildings. The phenomena of radon entry into and transport within these buildings may be quite different than in houses due to their greater heights, the existence of mechanical ventilation systems and vertical shafts, and the multizone nature of the airflows. In order to model radon in large buildings, a very simple source model was used to model radon entry through the foundation. This model is based on the assumption that the radon entry rate is dependent on the pressure difference between the basement floor and the outdoors. Specifically, the radon entry rate is equal to a radon entry coefficient multiplied by this pressure difference raised to the power *n*. This model is described in more detail in Persily (1993). The value of the radon entry coefficient used in these simulations is 0.02 Bq/s·Pa per m^2 of basement floor area, and the pressure exponent is assumed to equal 1.0. This radon source term was determined from CONTAM88 simulations of a two-story house with typical airtightness values in which the source term was varied until the indoor radon concentration was roughly 100 Bq/m^3. The radon source model also requires an air leakage coefficient for the airflow path from the basement floor through the soil and to the outdoors. A 4 Pa leakage area of 0.0085 cm^2 per m^2 of basement floor area, with a pressure exponent of 1.0, is used in these simulations. This radon entry model is obviously an oversimplified representation of an extremely complex phenomenon. It does not include such important parameters as soil radium content and permeability, temporal and spatial variations in these parameters, and the nature and extent of the cracks in the building-soil boundary. Therefore, the predicted radon concentrations should not be considered in absolute terms as indicative of expected concentrations in real buildings. Rather they should be considered relative to each other as a means of examining the impact of various parameters affecting radon in large buildings, such as weather conditions, building features, and ventilation system operation.

Computer simulations of radon transport in these four large buildings were performed using CONTAM88 by adding a so-called "soil zone" beneath the lowest building zone. This soil zone is connected to the lowest building zone by a minimal airflow resistance and connected to the outdoors by an airflow resistance equal to the basement floor area multiplied by 0.0085 cm^2/m^2. The outdoor radon concentration was assumed to equal 10 Bq/m^3 in all of the simulations. Steady-state indoor radon concentrations were calculated in each of the building zones based on the airflow rates calculated for a given set of weather conditions and ventilation system airflow rates. CONTAM88 also calculates the pressure difference from the bottom of the basement floor to the outdoors and the airflow rate from the outdoors to the basement through the basement floor. This last parameter can be combined with the predicted radon concentration in the soil zone to determine the radon entry rate into the building.

SIMULATION RESULTS

This section presents the results of selected calculations of airflow rate and radon concentrations in the four buildings using CONTAM88. The effects of weather conditions and the operation of exhaust fans in the individual apartments were examined for the apartment building. Building air change rates were calculated for three levels of outdoor air intake and a range of outdoor temperatures and wind speeds for the two office buildings. Air change rates were calculated for a range of weather conditions in the school building. The results of the airflow simulations are airflow rates through every opening in the exterior envelope and the interior partitions. CONTAM88 summarizes these airflow rates as infiltration, exfiltration, and intake and exhaust rates for the building. The infiltration and exfiltration rates are totals of the airflow rates into and out of the exterior envelope openings. The total intake rate is the sum of the infiltration rate through the building envelope and the outdoor airflow rate into the building through the ventilation systems. The total exhaust rate is the sum of the exfiltration rate through the envelope and the airflow rate out of the building through mechanical exhaust systems and other air handlers. CONTAM88 also calculates the airflow rate to and from any pair of zones for which such an interzonal airflow exists. The results are presented in this section primarily as whole building infiltration and intake rates. In large buildings, there are many interzonal airflow rates, and it is difficult to present them in either graphical or tabular form. All these airflow rates, however, are given in the CONTAM88 output files. The results of the radon modeling are presented for the four buildings for a limited number of cases. The results of the radon simulations that are presented include the pressure difference across the basement floor, the rate of radon entry into the building, and the radon concentrations in selected building zones.

Apartment Building

Airflow rate calculations were performed in the 12-story apartment building for a range of weather conditions. Calculations were also performed with a 47 L/s exhaust fan operating in each apartment.

Figure 5 shows the calculated airflow rates between each zone and the outdoors for the apartment building at a

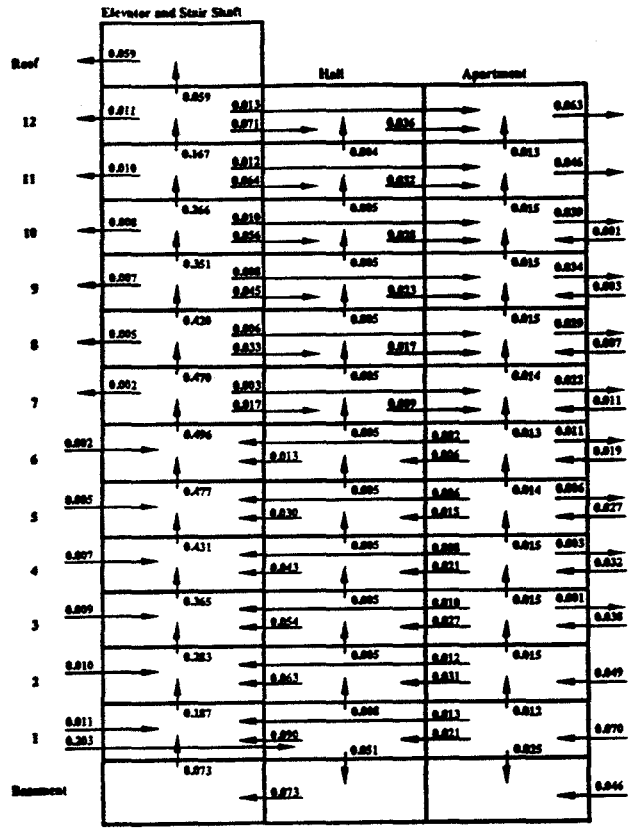

All flows are in kg/s.
The indoor-outdoor temperature difference is 20 °C and the wind speed is 0 m/s.

Figure 5: Airflow rates in apartment building.

temperature difference of 20°C and a wind speed of 0 m/s. Figure 6 shows the results with the exhaust fan operating in each apartment. In both figures, the flow rates between each type of zone (shaft, hall, and apartment) and between each zone type and the outdoors are given in kg/s. The symmetry of these buildings—and the fact that the elevator and stair shaft leakage is identical—allows the results to be depicted in graphical form. As seen in Figure 5, the upward flow of air in the stair and elevator shafts due to the stack effect is a dominant mechanism for air movement within the building. Air flows into the shafts from the outdoors, basement, hallways, and apartments for floors 1 through 6 and out of the shafts into the apartments and hallways on floors 7 and higher. Outdoor air infiltrates into the apartments on levels 1 through 10 (indicated by the outdoor-to-indoor arrows on the right side of Figure 5), and air exfiltrates from the apartments on levels 3 through 12 (indicated by the indoor-to-outdoor arrows in the figure). Note that the existence of both infiltration and exfiltration in the apartment on floors 3 through 10 indicates that there is a local neutral pressure level between the ceiling and floor of these apartments. The existence of multiple neutral pressure levels in a building depends on the relative airtightness of the exterior walls, floors, and vertical shaft walls and is discussed in Tamura and Wilson (1967).

Comparing Figures 5 and 6, it can be seen that the exhaust fans result in an overall reduction in the interior pressure of the building, which leads to increased infiltration of outdoor air, decreased exfiltration, and the shifting upward of neutral pressure levels. The location of the neutral pressure level for the shafts is indicated by a change in direction of the arrows on the left side of Figures 5 and 6. As indicated in Figure 5, without the exhaust fans, the neutral pressure level of the shafts is between floors 6 and 7, but with the fans (Figure 6), it is raised to an elevation between floors 7 and 8.

With the exhaust fans operating, the indoor-to-outdoor arrows on the right side of Figure 6 indicate airflow out of the apartments on floors 1 through 12. For floors 1 through 7, this airflow is exclusively the specified exhaust airflow rate of 0.057 kg/s, but on floors 8 through 12, additional outflow due to leakage is indicated by the fact that the airflow rates are greater than 0.057 kg/s. For example, on floor 11 the total airflow rate out of the apartments of 0.067 kg/s includes the exhaust component and an exfiltration component of 0.010 kg/s. The outdoor-to-indoor arrows on the right side of Figure 6 indicate that there is infiltration into the apartments on all floors of the building.

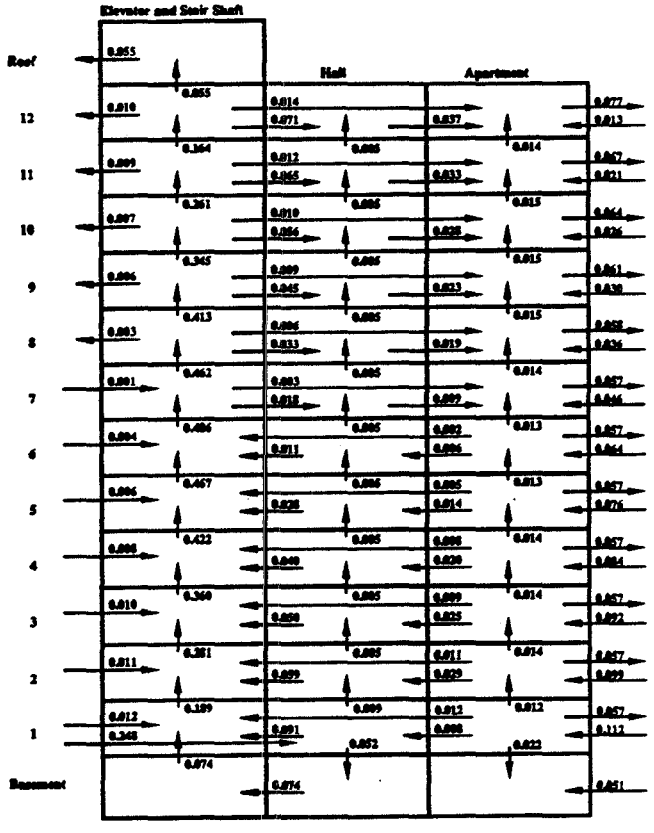

All flows are in kg/s.
The indoor-outdoor temperature difference is 20 °C and the wind speed is 0 m/s.

Figure 6: Airflow rates in apartment building with exhaust fans.

For a temperature difference of 20°C and a wind speed of 0 m/s, the whole building air change rate is 0.16 air changes per hour (ACH) without the exhaust fans operating and 0.38 ACH with the exhaust fans. In both cases, these air change rates are due to outdoor air flowing into the building through leaks in the exterior envelope.

Whole building air change rates were predicted as a function of weather conditions in the apartment building, both with and without the exhaust fans operating. The range of weather conditions included indoor-outdoor temperature differences from -10°C to 30°C in 5°C increments and wind speeds from 0 to 10 m/s in 2 m/s increments. The calculated air infiltration rates of the building with exhaust fans off is plotted against the indoor-outdoor temperature difference for a variety of wind speeds in Figure 7. For a wind speed of 0 m/s, there is a significant dependence of infiltration on temperature difference for the case with no exhaust fans. At higher wind speeds, or with the exhaust fans operating, temperature difference has little influence on the infiltration rate.

Office Building No. 1

Airflow rates were calculated for Office Building No. 1 for three cases of outdoor air intake and a range of weather conditions. At an indoor-outdoor temperature difference of 20°C and a wind speed of 0 m/s, the total outdoor air change rate was calculated to be 3.34, 1.68, and 0.66 ACH, respectively, for outdoor air intake rates of 100%, 50%, and minimum. These building air change rates are dominated by the outdoor air intake through the mechanical ventilation systems. The air infiltration rate through the exterior envelope is only 0.03 ACH in all three cases. The infiltration rate is small because the airflow rate of outdoor air into the building through the air handlers is significantly larger than the airflow rate out of the building through mechanical exhaust. This difference between the total outdoor air intake and exhaust airflow rates for the building causes the building to be at a positive pressure relative to the outdoors and limits the amount of envelope infiltration. The various mechanical ventilation airflow rates were input into the model such that the difference between the outdoor air intake and exhaust airflow rates for the building were the same for all levels of outdoor air intake. In a real building, the airflow rates may not be controlled so precisely.

The building airflow rates were calculated at all three levels of outdoor air intake for the same values of wind speed and temperature difference as were applied to the apartment building. The predicted envelope infiltration rates of the whole building for the 100% intake case are plotted against the inside-outside temperature difference for six different wind speeds in Figure 8. In all cases, the envelope infiltration rates are very small, on the order of 0.1 air changes per hour. For low wind speeds, the infiltration rates increase with an increase in temperature difference. For high values of wind speeds, the strength of the stack effect diminishes relative to the wind pressures acting across the exterior surfaces. As mentioned above, the predicted envelope infiltration rates are essentially independent of the level of outdoor air intake.

Figure 9 shows the calculated values of the total outdoor air change rate of the building, infiltration plus air handler intake. The air change rates are plotted against indoor-outdoor temperature difference for wind speeds of 0 and 8 m/s for all three levels of outdoor air intake. As seen in the figure, the air change rate decreases slightly as the temperature difference increases (outdoor temperature decreases) because the specific volume of the outdoor air depends on

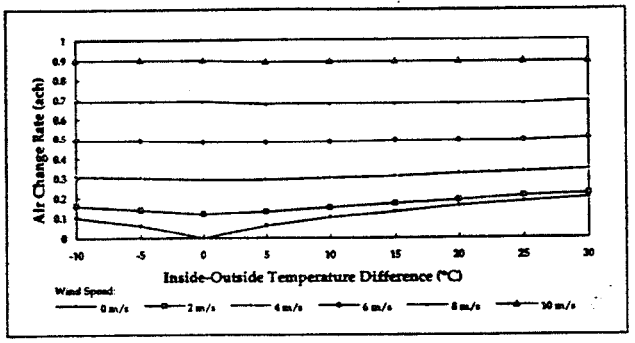

Figure 7: Air change rates of apartment building.

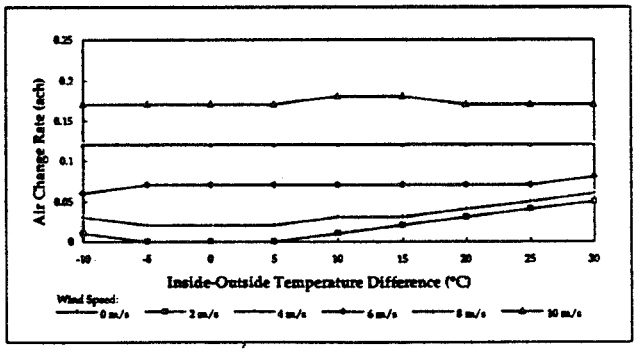

Figure 8: Air infiltration rates of office building No. 1 with 100% outdoor air.

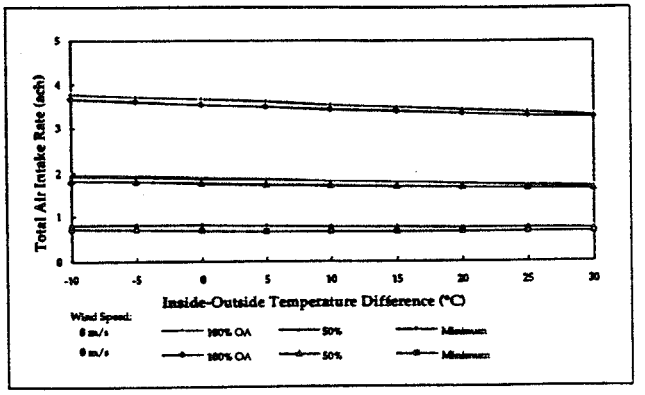

Figure 9: Total air intake rates of office building No. 1.

temperature. Otherwise, the air change rates vary little with weather.

The actual building on which Office Building No. 1 is based was subjected to tracer gas decay measurements of whole building air change rates (Persily et al. 1992). The results of these measurements were air change rates of about 0.3 ACH at minimum outdoor air intake and 2.6 ACH at maximum outdoor air. The values predicted using CONTAM88 with no wind and a 20°C temperature difference were 0.66 and 3.34 ACH for minimum and 100% intake, respectively. However, the predictions assume ideal control of the ventilation system airflow rates and are based on assumed values for many air leakage parameters. Also, it is not clear whether the maximum level of outdoor air intake for the real building's ventilation systems actually corresponds to 100% outdoor air intake.

Office Building No. 2

Airflow rates were calculated for Office Building No. 2 for three cases of outdoor air intake and the same range of weather conditions that was applied to the other buildings. At an indoor-outdoor temperature difference of 20°C and a wind speed 0m/s, the total outdoor air change rate was calculated to be 3.12, 1.56, and 0.15 ACH, respectively, for outdoor air intake rates of 100%, 50%, and minimum. The envelope infiltration rate is less than 0.01 ACH for 50% and 100% outdoor air intake and 0.05 ACH for minimum outdoor air intake. The infiltration rate is higher at the minimum condition because of differences in the balance of the outdoor air intake and the mechanical exhaust airflow rates at minimum intake compared to the balance at the other two intake values.

The predicted envelope infiltration rates of the whole building for the 100% intake case are plotted against the indoor-outdoor temperature difference in Figure 10. There is almost no dependence of the infiltration rate on temperature differences because the outdoor air change rate is dominated by the mechanical system intake.

Figure 11 is a plot of calculated total air intake rates as a function of the indoor-outdoor temperature difference. The total air intake rate is equal to the flow rate of outdoor air brought into the building by mechanical ventilation plus the air infiltration rate through building envelope. The air change rates at three levels of outdoor air intake are plotted against indoor-outdoor temperature difference for wind speeds of 0 and 10 m/s. As seen in the figure, the air change rate decreases as the temperature difference increases (outdoor temperature decreases) because the specific volume of the outdoor air depends on temperature.

The actual building on which Office Building No. 2 is based was also subjected to tracer gas decay measurements of whole building air change rates (Grot et al. 1989). The results of these measurements were air change rates of about 0.2 ACH at minimum outdoor air intake and 2.6 ACH at maximum outdoor air. The predicted values for Office Building No. 2 with no wind and a 20°C temperature difference were 0.15 and 3.12 ACH for minimum and 100% intake. As in the case of Office Building No. 1, these predictions assume ideal control of the ventilation system airflow rates and are based on assumed values for many air leakage parameters. Also, the maximum outdoor air intake in the real building may not be 100% outdoor air intake.

School Building

Airflow rates were calculated for the school building for the same range of weather conditions that was applied to the other buildings. Figure 12 is plot of the building infiltration and intake rates against indoor-outdoor temperature difference for a wind speed of 0 m/s. These infiltration rates vary only slightly with temperature difference, from 1.76 to 2.02 ACH, because the pressure differences caused by the operation of the mechanical ventilation system dominate the pressures from stack and wind. The total air intake rate is also relatively constant, but it decreases with increasing indoor-outdoor temperature difference due to the change in air density with air temperature. The total air intake rate of

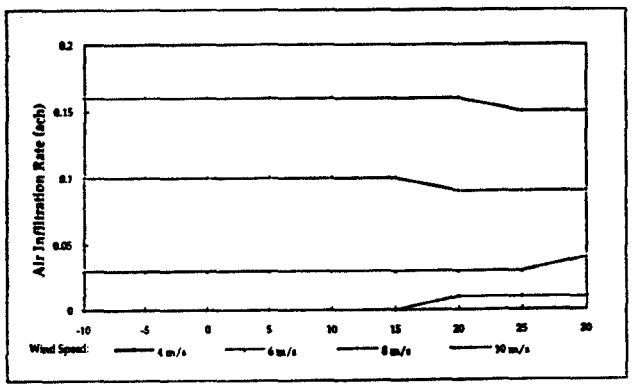

Figure 10: Air infiltration rates of office building No. 2.

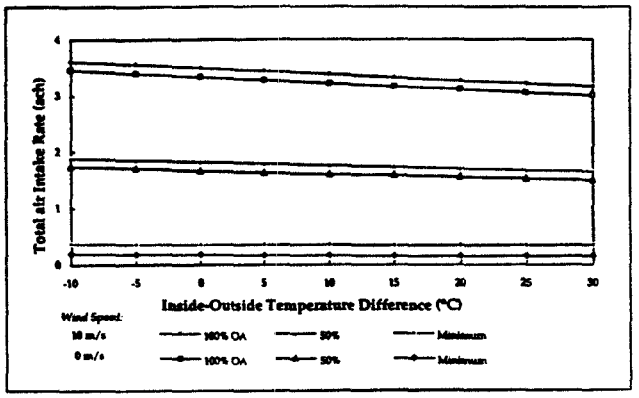

Figure 11: Total air intake rates of office building No. 2.

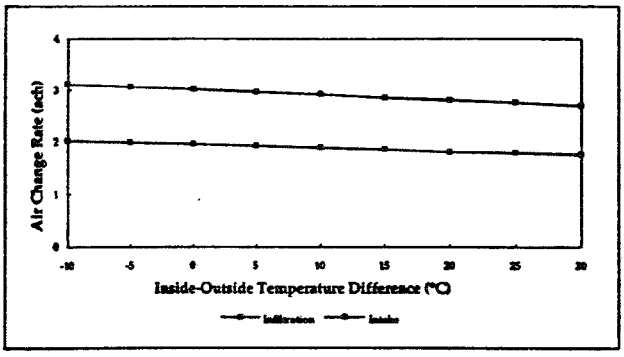

Figure 12: Air infiltration and total air intake rates of school building.

the building is constant because the outdoor air intake through the mechanical system dominates over stack- and wind-induced infiltration. Although it is not shown in the figure, neither the infiltration nor the intake rates vary with wind speed.

Results of Radon Simulations

This section presents the results of the radon simulations in the four buildings for a limited number of cases of weather conditions and other parameters. Tables 1 through 5 contain results for the apartment building. In each table, the second column is the predicted whole building air change rate and the third column is the predicted pressure difference between the basement floor and the outdoors. The fourth column is the radon entry rate into the basement. The last four columns contain the radon concentration for the given conditions in the basement, the average radon concentration for the second and twelfth floor apartments, and the average concentration for all of the apartments in the building. Table 1 shows the results with no wind for indoor-outdoor temperatures differences of -10°C, 0°C, 10°C, 20°C, and 30°C. For temperature differences less than or equal to zero, no radon enters the basement from the soil zone. For a positive temperature difference, the basement depressurization and the radon entry rate increase with temperature difference due to the stack effect. These increases result in increased radon concentrations for the twelfth-story apartments and the building average. No radon ever reaches the second floor apartments due to stack-driven flow from the basement and lower floors into the elevator and stair shafts and out of these shafts into the upper floors. The second-floor radon concentrations are greater than the outdoor concentration of 10 Bq/m^3 for a temperature difference of _10°C and less than 10 Bq/m^3 for positive temperature differences because of the density differences between the indoor and outdoor air.

Tables 2 through 4 contain the predicted radon concentrations for the apartment building as a function of wind

TABLE 1
Radon Simulation Results for Apartment Building, Wind Speed = 0 m/s

T_{in}-T_{out}, °C	Building Air Change Rate, h^{-1}	Basement Pressure, Pa	Radon Entry Rate, Bq/s	Radon Concentration, Bq/m^3 Basement	2nd Floor Apartments	12th Floor Apartments	Average of All Apartments
-10	0.10	4.5	0	10.3	10.3	10.3	10.3
0	0.0	0.0	0	10.0	10.0	10.0	10.0
10	0.10	4.8	69	874	9.7	141	63.9
20	0.16	-9.8	140	1130	9.3	180	78.0
30	0.20	-15.0	215	1320	9.0	209	89.9

TABLE 2
Radon Simulation Results for Apartment Building, T_{in}-T_{out} = -10°C

Wind Speed, m/s	Building Air Change Rate, h^{-1}	Basement Pressure, Pa	Radon Entry Rate, Bq/s	Radon Concentration, Bq/m^3 Basement	2nd Floor Apartments	12th Floor Apartments	Average of All Apartments
0	0.10	4.5	0	10.3	10.3	10.3	10.3
2	0.16	4.3	0	10.3	10.3	10.3	10.3
4	0.31	3.3	0	10.3	10.3	10.3	10.3
6	0.49	1.3	0	10.3	10.3	10.3	10.3
8	0.69	-1.4	21	235	11.1	10.3	11.8
10	0.90	-5.1	73	705	12.2	10.3	14.5

speed for indoor-outdoor temperature differences of -10°C, 0°C, and 10°C. As illustrated in Table 2, no radon enters into the building for a temperature difference of -10°C until the wind speed reaches 8 m/s. At lower wind speeds, the stack effect tends to pressurize the basement, keeping the basement at a positive pressure relative to the soil zone. The wind tends to depressurize the buildings, and at higher wind speeds, the wind-induced depressurization dominates the downward airflow from the stack effect and the basement becomes depressurized. For a temperature difference of 0°C, as shown in Table 3, radon enters the basement for wind speed greater than 0 m/s due to the wind-induced depressurization. Basement depressurization, the radon entry rate, the radon concentrations in the basement and second-story apartments, and the overall building average concentration all increase with wind speed. However, radon does not reach the twelfth floor at any wind speed.

At a temperature difference of 10°C, radon enters the basement at all wind speeds, and the entry rate increases with wind speed, as shown in Table 4. Radon from the soil appears on the second floor at a wind speed of 8 m/s due to wind-induced depressurization of that floor. Twelfth-floor radon concentrations and the average of all apartments decrease with increased wind speed due to increased dilu-

TABLE 3

Radon Simulation Results for Apartment Building, T_{in}-T_{out} = 0°C

Wind Speed, m/s	Building Air Change Rate, h^{-1}	Basement Pressure, Pa	Radon Entry Rate, Bq/s	Radon Concentration, Bq/m^3 Basement	2nd Floor Apartments	12th Floor Apartments	Average of All Apartments
0	0.0	0.0	0	10.0	10.0	10.0	10.0
2	0.12	-0.4	6	643	11.2	10.0	13.3
4	0.29	-1.7	24	1020	12.3	10.0	14.8
6	0.48	-3.8	54	1350	13.5	10.0	16.1
8	0.69	-6.7	95	1650	14.7	10.0	17.5
10	0.90	-10.4	149	1950	15.7	10.0	18.8

TABLE 4

Radon Simulation Results for Apartment Building, T_{in}-T_{out} = 10°C

Wind Speed, m/s	Building Air Change Rate, h^{-1}	Basement Pressure, Pa	Radon Entry Rate, Bq/s	Radon Concentration, Bq/m^3 Basement	2nd Floor Apartments	12th Floor Apartments	Average of All Apartments
0	0.10	-4.8	69	874	9.7	141	63.9
2	0.15	-5.1	74	979	9.7	120	52.7
4	0.30	-6.6	95	1530	9.7	108	51.0
6	0.48	-9.2	132	3040	9.7	91.5	45.6
8	0.68	-12.3	176	2970	15.0	43.1	35.9
10	0.89	-16.1	231	2920	30.4	18.9	33.3

TABLE 5

Radon Simulation Results for Apartment Building with Exhaust Fans, Wind speed = 0 m/s

T_{in}-T_{out}, °C	Building Air Change Rate, h^{-1}	Basement Pressure, Pa	Radon Entry Rate, Bq/s	Radon Concentration, Bq/m^3 Basement	2nd Floor Apartments	12th Floor Apartments	Average of All Apartments
-10	0.39	3.4	0	10.3	10.3	10.3	10.3
0	0.36	-1.1	15	804	10.0	10.0	17.1
10	0.36	-6.0	87	1070	9.7	116	42.7
20	0.38	-11.2	160	1280	9.3	164	61.2
30	0.41	-16.6	238	1440	9.0	196	74.2

tion with outdoor air. At low wind speeds, the small stack effect drives radon up to the twelfth floor. At higher wind speeds, the outdoor air change rate increases the dilution of the radon that reaches the upper floors.

Table 5 shows the results for the apartment building with a 47 L/s exhaust fan operating in each apartment for a range of indoor-outdoor temperatures and with no wind. No radon from the soil zone enters the building at the negative temperature difference. For positive temperature differences, the basement depressurization and the radon entry rate increase with temperature difference due to the stack effect. These increases result in increased radon concentrations for the twelfth-story apartments and the average of all apartments. However, no radon from the soil zone reaches the second-story apartments at any temperature difference due to the stack-driven airflow patterns. Radon entry rate is higher than corresponding cases with no exhaust fan (see Table 1), but the operation of the exhaust fans increases the outdoor air change rates, resulting in lower radon concentrations in the building.

Tables 6 and 7 show the predicted radon concentrations for Office Building No. 1 at minimum outdoor intake for no wind under a range of temperature differences and for wind speeds varying from 0 to 10 m/s with a temperature difference of 10°C. These tables show the radon concentrations in the lowest basement level, in the first and fifth floor occupied space, and for the whole building average. As seen in Table 6, no radon enters from the soil zone for temperature differences less than or equal to zero. For positive temperature differences, basement depressurization and radon entry increase with temperature difference due to the stack effect. These increases result in higher radon concentrations on the fifth floor and the average of all occupied spaces. No radon from the soil zone ever reaches the first-floor occupied space at any temperature difference. As seen in Table 7, radon enters the building at all wind speeds at this positive temperature difference, but the radon entry rate and the radon concentrations decrease with wind speed as basement depressurization decreases in absolute value.

Tables 8 and 9 shows the predictions for Office Building No. 2 with minimum outdoor air intake and the garage exhaust fans operating. Table 8 presents the results with no wind as a function of temperature difference. Radon from the soil zone enters the underground garage at all temperature differences due to the garage depressurization induced by the exhaust fans. The radon entry rate and the garage concentration increase with temperature difference due to the stack effect. Radon from the soil zone does not reach the first and seventh floors until the temperature difference is greater than 10°C. Table 9 shows the predictions as a

TABLE 6

Radon Simulation Results for Office Building No. 1, Wind speed = 0 m/s, Minimum Outdoor Air

T_{in}-T_{out}, °C	Building Air Change Rate, h^{-1}	Basement Pressure, Pa	Radon Entry Rate, Bq/s	Radon Concentration, Bq/m^3			
				Basement	1st Floor	5th Floor	Average of All Floors
-10	0.71	8.0	0	10.3	10.3	10.3	10.3
0	0.67	1.7	0	10.0	10.0	10.0	10.0
10	0.66	-4.1	369	209	9.7	14.4	39.4
20	0.66	-10.1	921	500	9.3	21.6	82.5
30	0.65	-16.8	1525	811	9.0	30.0	129

TABLE 7

Radon Simulation Results for Office Building No. 1, T_{in}-T_{out} = 10°C, Minimum Outdoor Air

Wind Speed, m/s	Building Air Change Rate, h^{-1}	Basement Pressure, Pa	Radon Entry Rate, Bq/s	Radon Concentration, Bq/m^3			
				Basement	1st Floor	5th Floor	Average of All Floors
0	0.66	-4.1	369	209	9.7	14.4	39.4
2	0.66	-4.0	368	209	9.7	14.4	39.4
4	0.68	-3.5	322	185	9.8	13.5	35.7
6	0.72	-2.3	212	125	9.8	11.7	26.7
8	0.77	-1.3	116	73.7	9.7	10.5	19.0
10	0.83	-0.4	34	28.2	9.7	9.9	12.4

TABLE 8

Radon Simulation Results for Office Building No. 2, Wind speed = 0 m/s, Minimum Outdoor Air

T_{in}-T_{out}, °C	Building Air Change Rate, h^{-1}	Basement Pressure, Pa	Radon Entry Rate, Bq/s	Radon Concentration, Bq/m³ Garage	Level B1	7th Floor	Average of All Floors
-10	0.19	-8.5	1358	35.0	10.4	10.3	10.3
0	0.17	-10.3	1655	40.1	10.0	10	10.0
10	0.16	-12.5	2006	46.6	9.7	9.7	9.7
20	0.15	-10.8	2368	51.7	10.8	16.0	14.8
30	0.15	-10.2	2736	57.6	10.2	18.7	16.9

TABLE 9

Radon Simulation Results for Office Building No. 2, T_{in}-T_{out} = 30°C, Minimum Outdoor Air

Wind Speed, m/s	Building Air Change Rate, h^{-1}	Basement Pressure, Pa	Radon Entry Rate, Bq/s	Radon Concentration, Bq/m³ Garage	Level B1	7th Floor	Average of All Floors
0	0.15	-17.0	2736	57.6	10.2	18.7	16.9
2	0.16	-18.1	2906	60.7	10.3	18.6	16.8
4	0.18	-21.2	3414	70.0	10.6	17.8	16.0
6	0.22	-26.5	4258	85.6	10.7	15.3	14.0
8	0.27	-33.8	5425	109	9.0	9.0	9.0
10	0.33	-43.2	6944	137	9.0	9.0	9.0

function of wind speeds at a temperature difference of 30°C. As indicated in the table, radon from the soil zone enters the garage at all wind speeds and its entry rate increases with wind speed. Radon reaches the B1 level and seventh floor for wind speeds less than 6 m/s, but at higher wind speeds, the occupied portion of the building is pressurized, preventing radon from flowing from the garage into the rest of the building.

The results for the school building are shown in Figure 13 at 50% outdoor air intake and no temperature difference or wind speed. This figure shows the radon concentration in each zone and the pressure difference between the floor of each zone and the outdoors. All but one of the building zones are depressurized by the ventilation system. At larger outdoor air intake rates, several of the building zones are positively pressurized, although several of the zones with exhaust vents only remain at a negative pressure relative to the outdoors. As the outdoor air intake percentage of the building ventilation system increases, the radon entry rate into each zone decreases or goes to zero and the radon concentrations in the building decrease. Wind tends to depressurize the building, pulling soil gas into the building and increasing radon entry rates and indoor radon concentrations.

SUMMARY

Building physical characteristics are described for a twelve-story multifamily residential building, two multistory office buildings with mechanical ventilation, and a one-story mechanically ventilated school building. Each of these buildings is idealized as a multizone building airflow system for calculations with CONTAM88. Selected computer simulations were performed to study the effects of various parameters, such as operations of building ventilation systems, wind speed, and indoor-outdoor temperature difference on building airflow rates and radon concentrations. It is acknowledged that the results of these simulations are based on many assumed input values and a simple model of radon entry. The reader is cautioned against generalizing these results to other situations pending additional model validation. Although experimental studies are needed to verify these predicted results, multizone models will play an increasing role in evaluating ventilation and indoor air quality in buildings.

ACKNOWLEDGMENTS

The radon modeling reported in this paper was supported by the U.S. Environmental Protection Agency under Interagency Agreement No. DW13935777-01-0.

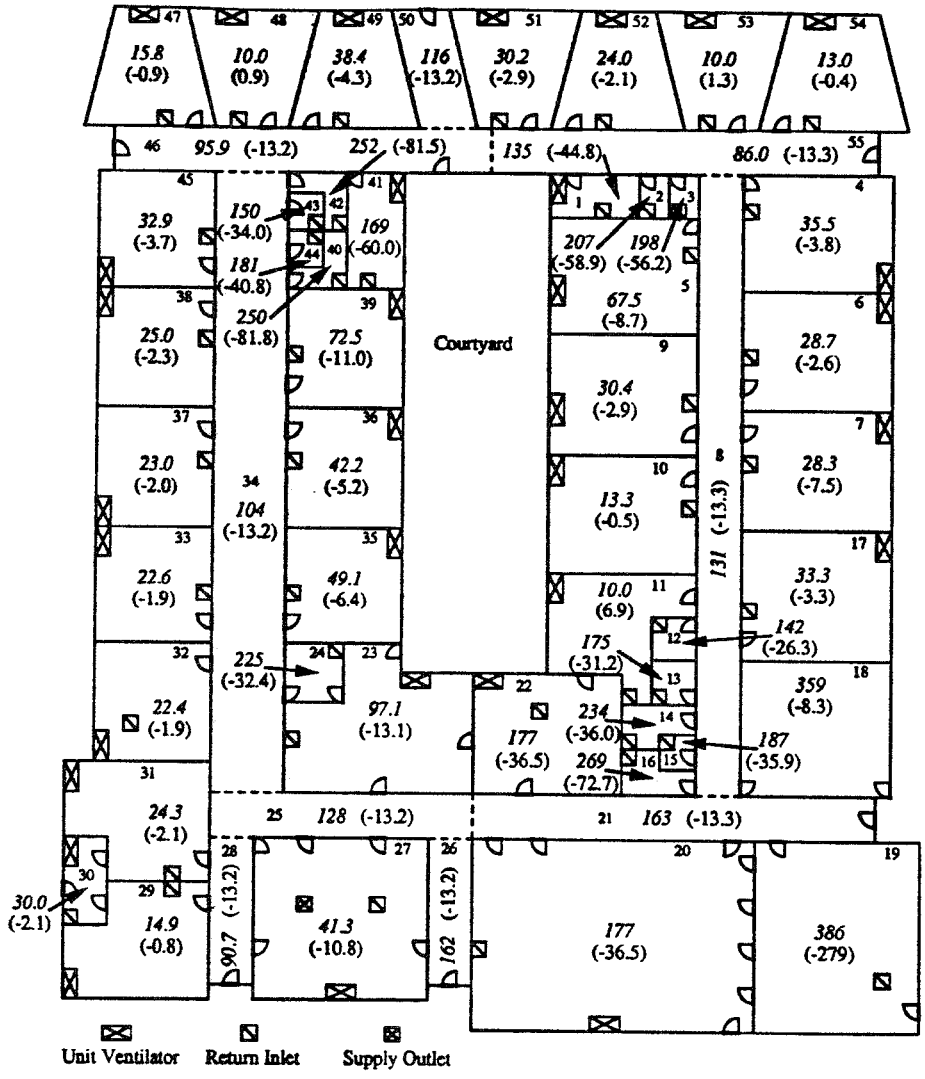

Radon concentrations in Bq/m³ for each zone are in *italics*.
Pressure differences in Pa between the floor of each zone and the outdoors are in parentheses.

Figure 13: Radon concentrations and zone pressures in the school building.

REFERENCES

Achakji, G.Y., and G.T. Tamura. 1988. Pressure drop characteristics of typical stairshafts in high-rise buildings. *ASHRAE Transactions* 94(1): 1223-1237.

ASHRAE. 1993. *1993 ASHRAE Handbook—Fundamentals*. Atlanta: American Society of Heating, Refrigerating and Air-Conditioning Engineers.

Austin, B.S., S.M. Greenfield, B.R. Weir, G.E. Anderson, and J.V. Behar. 1992. Modeling the indoor environment. *Environmental Science and Technology* 26(5): 851-858.

Axley, J. 1988. Progress toward a general analytical method for predicting indoor air pollution in buildings—Indoor air quality modeling Phase III report. NBSIR 88-3814, National Bureau of Standards, Gaithersburg, MD.

Dols, W.S., and A.K. Persily. 1992. A study of ventilation measurement in an office building. NISTIR 4905, National Institute of Standards and Technology, Gaithersburg, MD.

Fang, J.B., and A.K. Persily. 1994. CONTAM88 building input files for multizone airflow and contaminant dispersal modeling. NISTIR 5440, National Institute of Standards and Technology, Gaithersburg, MD.

Feustel, H.E., and V.M. Kendon. 1985. Infiltration models for multicellular structures—A literature review. *Energy and Buildings* 8: 123-136.

Feustel, H.E., and J. Dieris. 1992. A survey of airflow models for multizone structures. *Energy and Buildings* 18: 79-100.

Grot, R.A., A.K. Persily, A.T. Hodgson, and J.M. Daisey. 1989. Environmental evaluation of the Portland East Federal Office Building preoccupancy and early occupancy results." NISTIR 89-4066, National Institute of Standards and Technology, Gaithersburg, MD.

Grot, R.A. 1991. User manual NBSAVIS CONTAM88. NISTIR 4585, National Institute of Standards and Technology, Gaithersburg, MD.

Haghighat, F. 1989. Air infiltration and indoor air quality models—A review. *International Journal of Ambient Energy* 10(3): 115-122.

Persily, A.K., W.S Dols, S.J. Nabinger, and S. Kirchner. 1991. Preliminary results of the environmental evaluation of the Federal Records Center in Overland, Missouri. NISTIR 4634, National Institute of Standards and Technology, Gaithersburg, MD.

Persily, A.K., W.S. Dols, and S.J. Nabinger. 1992. Environmental evaluation of the Federal Records Center in Overland, Missouri. NISTIR 4883, National Institute of Standards and Technology, Gaithersburg, MD.

Persily, A.K. 1993. Modeling radon transport in multi-story residential buildings. *Modeling of Indoor Air Quality and Exposure*, ASTM STP 1205, Niren L. Nagda, ed., pp. 226-242. American Society for Testing and Materials, Philadelphia, PA,

Said, N.A. 1988. A review of smoke control models. *ASHRAE Journal* 30(4): 36-40.

Tamura, G.T., and A.G. Wilson. 1967. Building pressures caused by chimney action and mechanical ventilation. *ASHRAE Transactions* 73(2): 2.1-2.8.

Walton, G.N. 1983. A computer algorithm for estimating infiltration and inter-room air flows. NBSIR 83-2635, National Institute of Standards and Technology, Gaithersburg, MD.

Walton, G.N. 1984. A computer algorithm for predicting infiltration and inter-room airflows. *ASHRAE Transactions* 90(1B): 601-610.

Walton, G.N. 1994. CONTAM93 user manual. NISTIR 5385, National Institute of Standards and Technology, Gaithersburg, MD.

APPENDIX A

Building Component Air Leakage Data Base

Multizone airflow modeling requires air leakage values for every significant opening in the exterior envelope and in interior partitions. Determining these air leakage values is difficult since the air leakage of an individual building element depends on its design, installation, and deterioration over time. The only way to know the air leakage characteristics of an element is to measure it. However, it is impractical to measure all the leakage characteristics of all openings in a building. In many cases, air leakage values from measurements on similar components can be used in airflow modeling. However, only limited measurements have been made in large buildings. This appendix presents air leakage values relevant to large buildings from the published literature.

The leakage characteristics of a building component can be measured by imposing a series of pressure differences across the component and measuring the airflow rate required to maintain each pressure difference. So-called component pressurization techniques are discussed in ASTM Standards E-283[A1] and E-783[A2] for measurements in the laboratory and field, respectively. Whole building pressurization testing involves pressurizing an entire building and measuring the airflow rate required to do so. The results of the measurements give the leakage characteristics for all the building leakage in combination. Whole building pressurization is described in ASTM Standard E-779[A3].

Over the years, a number of component and whole building pressurization tests have been conducted in large commercial buildings. This appendix is the result of a literature search of leakage data in large public and commercial buildings published after 1970. There is a significant amount of leakage data on single-family residential buildings, for example in Chapter 23 of *ASHRAE Fundamentals*[A4]. This appendix is limited to data from larger commercial buildings.

The appendix presents the leakage data in tabular form, organized by building component and building type. The first column in the table is the effective leakage area at a reference pressure of 4 Pa and a discharge coefficient of 1.0. The next column contains a brief description of the component. The third column states whether the leakage area is based on a component leakage test (C) or is derived from a whole building pressurization test (WB). The last column is the reference for the data.

The air leakage data in the literature is reported in a variety of different forms including leakage areas and leakage coefficients of a variety of reference pressures and discharge coefficients. In the table, all air leakage values are presented as effective leakage areas using a reference pressure difference of 4 Pa and a discharge coefficient of 1.0. The effective leakage areas in the table were converted from the reported form using the formulas in Chapter 23 of *ASHRAE Fundamentals* [A4].

TABLE A1
Effective Leakage Area (in cm^2/m^2) of Building Components

ELA at 4 Pa	Component Description	Basis	Reference No.
Exterior Walls - Office Buildings			
3.64	Precast concrete panel	WB	A5

ELA at 4 Pa	Component Description	Basis	Reference No.
2.74	Precast concrete panel walls retrofitted with rigid insulation after about 20 years WB	WB	A6
1.63	Precast concrete panel	WB	A5
1.02	Precast concrete panel walls retrofitted with all windows and vertical columns recaulked after about 20 years	WB	A6
0.55	Precast concrete panel	WB	A5
1.91	Metal panel	WB	A5
1.08	Metal panel walls retrofitted by replacing metal panel with a curtain wall cladding system after about 20 years	WB	A6
1.36	Metal panel	WB	A5
1.36	Metal panel walls retrofitted with all joints in the curtain wall recaulked after about 20 years	WB	A6
1.30	Precast concrete panel	WB	A5
1.60	Precast concrete panel walls after about 20 years	WB	A6
1.87	Precast concrete panel	WB	A5
1.35	Precast concrete panel walls retrofitted by installing a new roof	WB	A6
0.50	Metal panel	WB	A5
2.10	Precast concrete panel	WB	A7
1.30	Tile veneer, concrete masonry backup	WB	A7
1.90	Stone panel	WB	A7
0.60	Brick veneer, concrete masonry backup	WB	A7
2.30	Brick veneer, steel stud backup	WB	A7
1.10	Brick veneer, brick backup	WB	A7
2.90	Precast concrete panel	WB	A7
5.20	Glass and metal curtain wall	WB	A8
4.97	Glass and metal curtain wall	WB	A9
2.53	Precast concrete panel	WB	A9
1.60	PEAC panel	WB	A10
1.00	Glass and metal curtain wall	WB	A10
0.53	Precast concrete panel	WB	A10
Exterior Walls - Apartment Buildings			
4.50	Brick veneer, concrete masonry backup	C	A11
2.70	Brick veneer, concrete masonry backup	C	A11
3.12	Masonry panel	WB	A12
1.13	Masonry panel	WB	A12
Exterior Walls - School Buildings			
6.7	Brick veneer, concrete masonry backup	WB	A13
4.8	Brick veneer, concrete masonry backup	WB	A13
2.9	Brick veneer, concrete masonry backup	WB	A13
Exterior Walls - Supermarkets and Shopping Malls			
15.7	Concrete block	WB	A14
9.20	Brick veneer, concrete masonry backup	WB	A14
2.60	Concrete block, steel stud backup	WB	A14
Floors - Office Buildings			
0.39	Reinforced concrete	C	A15
0.26	Reinforced concrete	C	A15
0.22	Reinforced concrete	C	A15
Floors - Apartment Buildings			
0.32	Not available	C	A11
0.26	Not available	C	A11
0.20	Not available	C	A11
0.12	Not available	C	A11
Interior Partition Walls - Apartment Buildings			
4.30	Gypsum board on stud wall	C	A11
1.90	Gypsum board on stud wall	C	A11
0.53	Gypsum board on stud wall	C	A11
Elevator Shaft Walls - Office Buildings			
7.50	Hollow clay tile block or concrete block	C	A16
3.50	Cast-in-place concrete	C	A16
0.75	Cast-in-place concrete	C	A16
Stairwell Walls - Office Buildings			
1.50	Cast-in-place concrete	C	A16
0.46	Cast-in-place concrete	C	A16
0.06	Cast-in-place concrete	C	A16

ELA at 4 Pa	Component Description	Basis	Reference No.
Elevator Doors - Office Buildings			
174	1.07 m wide x 2.13 m high, with a crack width of 6.8 mm	C	A16
145	1.07 m wide x 2.13 m high, with a crack width of 5.8 mm	C	A16
62	1.07 m wide x 2.13 m high, with a crack width of 5.3 mmC	C	A16

REFERENCES

A1. ASTM. 1991. *Standard E-283, Standard test method for determining the rate of air leakage through exterior windows, curtain walls, and doors under specified pressure differences across the specimen.* Philadelphia: American Society for Testing and Materials.

A2. ASTM. 1991. Standard E-783, Standard test method for field measurement of air leakage through installed exterior windows and doors. Philadelphia: American Society for Testing and Materials.

A3. ASTM. 1992. Standard E-779, Standard test method for determining air leakage rate by fan pressurization. Philadelphia: American Society for Testing and Materials.

A4. ASHRAE. 1993. *1993 ASHRAE Handbook—Fundamentals*. Atlanta: American Society of Heating, Refrigerating and Air-Conditioning Engineers.

A5. Tamura, G.T., and C.Y. Shaw. 1976. Studies on exterior wall air tightness and air infiltration of tall buildings. *ASHRAE Transactions* 82(1): 122-134.

A6. Shaw, C.Y., J.T. Reardon, and M.S. Cheung. 1993. Changes in air leakage levels of six Canadian office buildings. *ASHRAE Journal* 35: 34-36.

A7. Persily, A.K., and R.A. Grot. 1985. The airtightness of office building envelopes. *Thermal Performance of Exterior Envelopes of Buildings III.* Atlanta: American Society of Heating, Refrigerating and Air-Conditioning Engineers, Inc.

A8. Persily, A.K., W.S. Dols, S.J. Nabinger, and S. Kirchner. 1991. Preliminary results of the environmental evaluation of the Federal Records Center in Overland, Missouri. NISTIR 4634, National Institute of Standards and Technology, Gaithersburg, MD.

A9. Perera, M.D.A.E.S., R.K. Stephen, and R.G. Tull. 1990. Airtightness measurements in two U.K. office buildings. *ASTM STP 1067, Air change rate and airtightness in buildings*, M.H. Sherman, ed., pp. 211-221. Philadelphia: American Society for Testing and Materials.

A10. Shaw, C.Y., D.M. Sander, and G.T. Tamura. 1973. Air leakage measurements of the exterior walls of tall buildings. *ASHRAE Transactions* 79(2): 40-48.

A11. Shaw, C.Y., R.J. Magee, and J. Rousseau. 1991. Overall and component airtightness values of a five-story apartment building. *ASHRAE Transactions* 97(2): 347-353.

A12. Shaw, C.Y., S. Gasparetto, and J.T. Reardon. 1990. Methods for measuring air leakage in high-rise apartments. *ASTM STP 1067, Air Change Rate and Airtightness in Buildings*, M.H. Sherman, ed., pp. 222-230. Philadelphia: American Society for Testing and Materials.

A13. Shaw, C.Y., and L. Jones. 1979. Air tightness and air infiltration of school buildings. *ASHRAE Transactions* 85(1): 85-95.

A14. Shaw, C.Y. 1981. Air tightness: Supermarkets and shopping malls. *ASHRAE Journal* 23: 44-46.

A15. Tamura, G.T., and C.Y. Shaw. 1978. Experimental studies of mechanical venting for smoke control in tall office buildings. *ASHRAE Transactions* 84(1): 54-71.

A16. Tamura, G.T., and C.Y. Shaw. 1976. Air leakage data for the design of elevator and stair shaft pressurization systems. *ASHRAE Transactions* 82(2): 179-190.